Adaptation of Schelkunoff's Superdirective Antenna Theory for the Realization of Superoscillatory Antenna Arrays

Alex M. H. Wong and George V. Eleftheriades, *Fellow, IEEE*

***Abstract*—We have adapted Schelkunoff's method of antenna pattern synthesis to the design of superoscillatory waveforms. Our method stems from the observation that superdirectivity and superoscillation are dual phenomena in the space and spectral domains; it can be applied to construct any periodic superoscillatory wave functions. Using this method, we designed two subwavelength focusing schemes—in free space and within a waveguide—at an image distance of five wavelengths. We first describe how we extend the concept of superdirectivity toward constructing superoscillatory waveforms, then provide in-depth formulations as they apply to each design example. We also report full-wave simulation results verifying subwavelength focusing to 0.6 times that of the diffraction limit at a distance five wavelengths away from the source.**

***Index Terms*—Diffraction limit, image resolution, subwavelength focusing, superdirectivity, superoscillation.**

I. Introduction

In the past decade, there has been considerable amount of work in focusing electromagnetic waves to dimensions below those allowed by the diffraction limit, with numerous intended applications including imaging, sensing, and lithography. Most of these works achieve focusing using evanescent waves [1], [2], which limits their focal lengths to the evanescent near field corresponding to distances typically less than half a wavelength from the focusing device. Clearly, it would be very desirable to have a subwavelength focusing device with a longer working focal length. One route to such a focusing device has recently been proposed [3], [4], making use of the concept of superoscillation. Superoscillation is a phenomenon whereby the delicate interference of *propagating* electromagnetic waves results in an overall waveform that, within a limited stretch of space, contains variations faster than the highest spatial frequency component of the electromagnetic wave involved. Since only propagating waves are involved: 1) the focusing is certainly of the subdiffraction type; and 2) the subwavelength focusing capability can be extended to much longer imaging distances—to several wavelengths and beyond.

In this work, we propose a method to synthesize superoscillatory waveforms by means of adapting from the theory of superdirective antennas. This adaptation allows us to: 1) design superoscillation waveforms using well-established analytical formulations; and 2) arrive at implementations that achieve significant focusing improvements over the diffraction limit while maintaining reasonable robustness, from which practical focusing devices can be built. We first review superdirective antennas, then view them in an alternate perspective that readily connects to superoscillations. Subsequently, we build upon this link and introduce a new approach to designing superoscillatory waveforms. We then demonstrate our approach by constructing superoscillatory waveforms in two environments—in free space and within a waveguide. For each case, we first analytically determine the required source excitation, and then provide full-wave simulation results verifying subwavelength focusing at an image distance of 5λ.

Manuscript received February 25, 2010; accepted March 29, 2010. Date of publication April 08, 2010; date of current version April 27, 2010. This work was supported by the Natural Sciences and Engineering Research Council of Canada.

The authors are with the Department of Electrical and Computer Engineering, University of Toronto, Toronto, ON M5S 3G4, Canada (e-mail: gelefth@waves.utoronto.ca).

Color versions of one or more of the figures in this letter are available online at http://ieeexplore.ieee.org.

Digital Object Identifier 10.1109/LAWP.2010.2047710

II. Theoretical Framework

A. Schelkunoff's Approach to Superdirectivity

It has been well known that one can represent the far field of an array of isotropic antennas using the array factor

$$f(\theta) = \sum_{n=0}^{N-1} a_n u^n, \quad \text{where } u = e^{-jkd\cos\theta}. \tag{1}$$

See Fig. 1(a) for a diagram of the array. Here, N is the number of elements in the array, a_n is the complex excitation coefficient for the nth element, and u represents the phase shift between adjacent array elements, which depends on the uniform element separation d, the spatial frequency k, and the angle of observation θ. Schelkunoff, in [5], recognized the right-hand side of (1) as a polynomial function $F(u)$ with $N-1$ zeros on the plane of complex u; $f(\theta)$ is then the value of $F(u)$ on a further restricted domain of real values of θ, which corresponds to an arc on the unit circle joining e^{-jkd} to e^{jkd}, as shown in Fig. 1(b) for $d = \lambda/4$. In antenna array theory , this restricted domain is called the visible region (VR) of the antenna array. Schelkunoff proposed to design the antenna pattern by appropriately placing zeros to achieve a desired profile for $F(u)$ along the VR.

A case of particular interest occurs when $d < \lambda/2$. Here, the VR subtends an angle less than 2π from the origin, and an invisible region (IR) exists, as shown in Fig. 1(b), along which the value of $F(u)$ does not affect $f(\theta)$. Hence, the zeros of the polynomial can be concentrated along the VR to obtain sharp variations. This gives rise to the concept of superdirectivity: By exciting an antenna array according to weights derived from the appropriate placement of zeros, one can form an arbitrarily sharp antenna beam with a fixed-size antenna array.

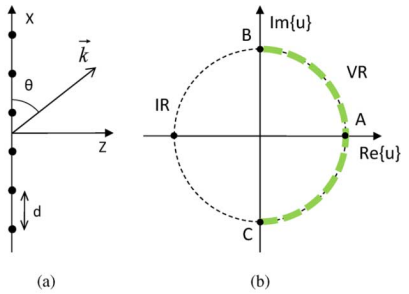

Fig. 1. (a) A diagram of an antenna array, with the element separation d, the beam observation angle θ, and the coordinate directions defined. (b) The plane of complex u, showing the visible region (VR, thick dashed curve) and the invisible region (IR) for an array with $d = \lambda/4$. The labeled points are A ($u = 1$), B ($u = e^{+jkd} = j$), and C ($u = e^{-jkd} = -j$).

B. Space-Spectral Perspective to Antenna Array Design

We now view Schelkunoff's process of antenna design from another perspective, which we subsequently adapt toward designing superoscillatory waveforms. We first write

$$g(x) = \sum_{n=0}^{N-1} a_n \delta(x - nd) \tag{2}$$

as the continuous excitation function for an array aligned along the x-axis. Since we consider an array of isotropic antennas, the far field corresponding to excitation $g(x)$ is given by its angular spectrum [6], which is found by a Fourier transform in the spatial domain

$$f(k_x) = \int_{-\infty}^{\infty} g(x) e^{-jk_x x} dx = \sum_{n=0}^{N-1} a_n e^{-jk_x nd}. \tag{3}$$

Keeping in mind that $k_x = k\cos\theta$, we see from (1) and (3) that $f(k_x) = f(\theta)$ for $k_x \leq k$ (i.e., within the VR). Thus, one can view $f(k_x)$ as an extension of $f(\theta)$: While $f(\theta)$ only describes propagating waves, $f(k_x)$ describes both propagating and evanescent waves. Furthermore, we can understand superdirectivity as a twofold process. First, the weights on an antenna array are designed to fine-tune its propagation spectrum, at the expense of tolerating an uncontrolled, often high-amplitude, evanescent spectrum. Then, in the far field, the propagation spectrum gets mapped into the antenna's radiation pattern, thus achieving superdirectivity. In this twofold process, only the latter step involves the far-field approximation; the initial step rests purely on a Fourier transform basis, which allows for handy extensions to other areas of interest.

C. From Superdirectivity to Superoscillation

Here, we build upon our perspective on superdirectivity to construct superoscillatory waveforms. To achieve this, we simply swap the space and spectral domains along the array axis ($x \leftrightarrow k_x$) to obtain

$$g(k_x) \xrightarrow{F.T.} f(x). \tag{4}$$

That is to say, N uniformly spaced spectral lines with weights $g[n]$ (excitation weights from a superdirective antenna) correspond to a spatial distribution with subwavelength peaks, which is precisely a superoscillatory waveform. Just as the superdirective antenna is a fixed-size antenna that can form an arbitrarily narrow beam, the superoscillatory waveform will be spectrally band-limited to include only propagating waves; nonetheless, it can still focus electromagnetic radiation to an arbitrarily small spatial width, given the presence and proper tuning of sufficiently many closely spaced spectral lines. The only caveat is that while the high-amplitude evanescent waves generated by superdirective antennas are invisible in the far field, the high-amplitude sidebands of a superoscillatory waveform appear along with the subwavelength peak. Indeed, high-amplitude sidebands have been proven to exist in all superoscillatory waveforms [7]. Notwithstanding their presence, the generated subwavelength superoscillation peak may still prove useful in many applications.

III. Construction of Superoscillatory Waveforms

We now apply the forgoing formulation to construct superoscillatory waveforms in two environments: in free space and in a waveguide. While for simplicity, we render all fields invariant in the y-direction and consider 1D electric field focusing in both designs, the principles we demonstrate here can be straightforwardly extended to 2D focusing in a 3D environment.

A. Free Space Superoscillatory Waveform

In this first example, we design a free space superoscillatory focusing device that generates, at the source plane, $N = 5$ spectral lines in the following form:

$$\widetilde{E}_{\rm src}(k_x) = \sum_{n=0}^{N-1} b_n \delta(k_x - n\Delta k - k_{x0}) \tag{5}$$

where $\Delta k = 2k/5$ is the uniform line spacing, and $k_{x0} = -4k/5$ marks the location of the first spectral line. Our task will be to find the coefficients b_n, which will allow us to form a subwavelength superoscillation peak at a distance of $s = 5\lambda$ away from the source.

We begin by adapting from an established method that designs a superdirective antenna through analytical expansion into a basis of Tschebyscheff polynomials [8], [9]. In light of our above formulation, we follow this same method to determine the set of zeros, w_{zn}, which yields an image waveform with the narrowest central peak width and constant sidelobes at 20% the central peak field strength (4% intensity) for a range of $\lambda/2$ on both sides of the peak. Fig. 2 shows the resultant zero locations and the corresponding spatial spectrum, $\widetilde{E}_{\rm img}(k_x)$, calculated as follows:

$$E_{\rm img}(x) = \prod_{n=1}^{N-1} (w - w_{zn}) = \sum_{n=0}^{N-1} a_n w^n,\ w = e^{-jx\Delta k} \tag{6}$$

$$\widetilde{E}_{\rm img}(k_x) = \sum_{n=0}^{N-1} a_n \delta(k_x - n\Delta k - k_{x0}). \tag{7}$$

Relating $\widetilde{E}_{\rm img}(k_x)$ to $\widetilde{E}_{\rm src}(k_x)$ in (5) through back propagation by the image distance s, we find b_n from (8)

$$\widetilde{E}_{\rm src}(k_x) = \widetilde{E}_{\rm img}(k_x) e^{+jk_z s} \Rightarrow b_n = a_n e^{+jk_z s}, \quad \text{where } k_z = -j\sqrt{k_x^2 - k^2}. \tag{8}$$

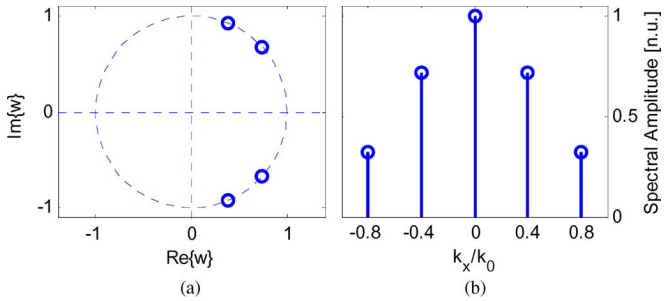

Fig. 2. (a) The location of zeros in the complex w plane for synthesizing a free space subwavelength superoscillatory waveform. (b) A plot showing amplitudes for the five spectral lines required to achieve superoscillation.

Finally, taking the inverse Fourier Transform of (5) gives us the desired spatial excitation function at the source plane

$$E_{\mathrm{src}}(x) = \frac{1}{2\pi} \sum_{n=0}^{N-1} b_n e^{j(k_{x0}+n\Delta k)x}. \tag{9}$$

We verify our results with a 2D full-wave simulation at 3 GHz using Comsol Multiphysics. Fig. 3(a) shows the simulated electric field distribution overlaid atop the computation domain. We excite a periodic electric field function $E_y(x) = E_{\mathrm{src}}(x)$ along the $z = 0$ plane and observe the subwavelength focus at $z = 5\lambda$. The simulation region is reduced to one period using periodic boundaries (implemented here by perfect magnetic conductors) in the x-direction. Fig. 3(b) shows a close up of the imaged electric field in the region $|x| \leq \lambda/2$, normalized alongside the source electric field and the diffraction-limited sinc function. While the waveform at the source plane contains no subwavelength variations, a subwavelength peak appears in the image whose full-width at half-maximum (FWHM) measures 0.37λ. This is greatly improved over the diffraction-limited sinc function's FWHM of 0.60λ even though the focal plane is located 5λ from the source. Fig. 3(c) shows that the simulated and calculated electric fields agree extremely well across the entire image plane and reveals that the subwavelength peak has an amplitude 6.6% that of the sidebands. In the following example, we shall demonstrate that this can be improved by using more spectral lines.

We stress that our obtained result differs from a superdirective antenna pattern based on two observations. First, whereas the source spectrum for a superdirective antenna contains high-amplitude evanescent components, our source spectrum entirely comprises propagating components, whose amplitudes are as shown in Fig. 2(b). Second, our simulated electric field amplitude, as shown in Fig. 3(a), has no angular dependence. This signifies that the focus does not reside in the far field and hence cannot be produced by superdirectivity, which is a far-field phenomenon.

B. Waveguide Superoscillatory Waveform

While operational, the above-introduced scheme might not be most suited for microwave implementations. This is because in order to produce the sharp lines in the spatial spectrum, one needs to extend the source plane excitation across many

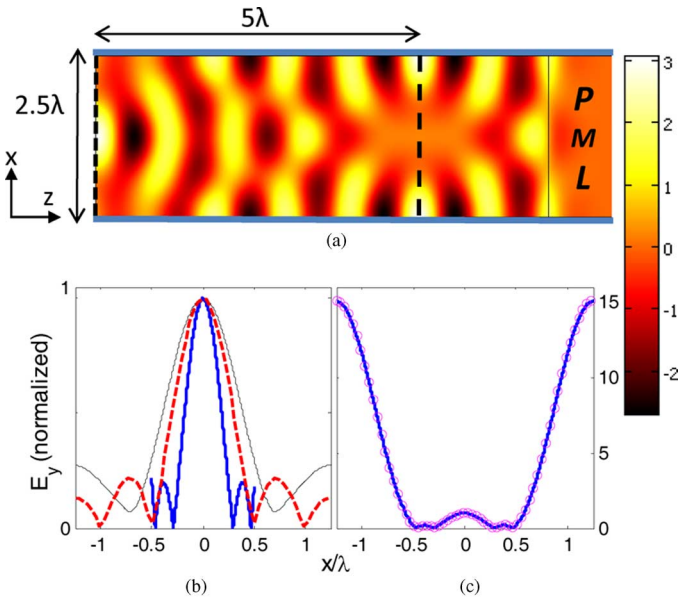

Fig. 3. Superoscillatory subwavelength electric field focusing in free space. (a) The simulated electric field distribution in 2D. Depicted geometries include the source plane (dotted, left side of the domain), the image plane (dashed, 5λ from the source), the absorptive termination (PML), and periodic (PMC) boundaries (thick lines in the $\pm x$-directions). (b) Electric field amplitude at the image plane, for the region $|x| \leq \lambda/2$ (thick solid line), compared alongside the field amplitude at the source plane (thin solid line), and the diffraction-limited sinc function (dashed line). (c) Electric field amplitude at the image plane, showing extremely well agreement between simulation (solid line) and theoretical calculation (circles).

wavelengths. This might lead to device apertures too large to be practically implemented. Instead, a waveguide provides a comparatively compact environment in which one can generate uniformly spaced spectral lines in the form of waveguide modes and thereby construct superoscillatory waveforms. Fig. 4(a) shows our proposed superoscillatory focusing scheme within a rectangular waveguide. We choose the waveguide cross section to be 3λ by $\lambda/3$, such that only the TE_{10}, TE_{30}, and TE_{50} propagating modes can be excited with an even excitation. Five y-directed line sources excite the waveguide at $z = 0$. They are spaced $\lambda/2$ apart, which is guaranteed sufficient by Nyquist's sampling criterion since here we only deal with propagating waves. We seek to feed these line sources with current weights $h[m]$, such that we excite the aforementioned modes in correct proportions to form a superoscillatory focus 5λ away from the sources.

This is clearly a very simple way to implement a subwavelength waveform. In the following, we complete our design by determining the weights $h[m]$. The three aforementioned modes give us $N = 6$ spectral lines spaced $\Delta k = k/3$ apart, whose amplitudes at the source plane can be designed in a manner very similar to what we introduced for the free space superoscillatory waveform. Having six spectral lines gives us freedom in placing five zeros on the complex w plane. We place four of the zeros at the same locations as shown in Fig. 2, and the remaining zero at $w_{z5} = -1$ to form nulls at the waveguide walls. With these zero locations, we follow (6) to (8) to find the spectral coefficients b_n at the source plane. The desired source plane spectrum is now described by (5). Since we seek to excite the waveguide with

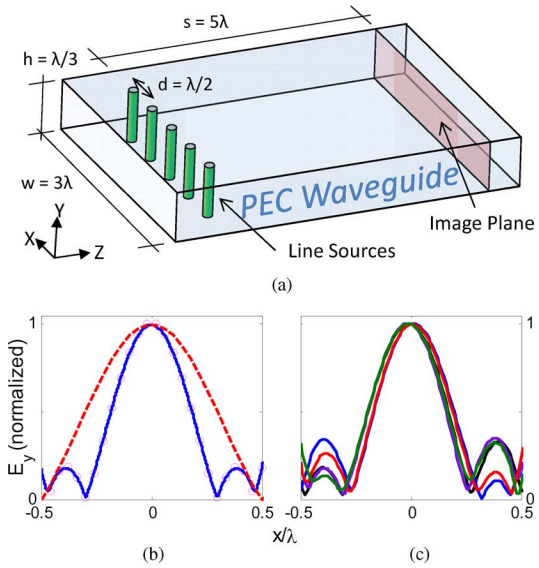

Fig. 4. Superoscillatory subwavelength electric field focusing in waveguide. (a) A diagram of the waveguide superoscillation focusing scheme showing the width and height of the waveguide, the excitation line sources, and the subwavelength focusing image plane. (b) The simulated electric field amplitude at the image plane for the region $|x| \leq \lambda/2$ (solid line), compared alongside theoretical calculation (circles) and the diffraction-limited sinc function (dashed line). (c) Typical electric field amplitude distributions across the image plane with 1% error in current excitations.

line source elements, we divide out the line source's spectral effect, $\widetilde{E}_{\text{elem}}(k_x) = 2/k_z = 2j/\sqrt{k_z^2 - k^2}$ [10], to obtain the desired array contribution to the source spectrum

$$\widetilde{E}_{\text{array,src}}(k_x) = \frac{\widetilde{E}_{\text{src}}}{\widetilde{E}_{\text{elem}}} = \sum_{n=0}^{N-1} b'_n \delta(k_x - n\Delta k - k_{x0}),$$
$$\text{where } b'_n = -\frac{j\left[b_n\sqrt{(k_{x0}+n\Delta k)^2 - k^2}\right]}{2}. \quad (10)$$

Finally we sample its inverse Fourier Transform to find $h[m]$.

$$E_{\text{array,src}}(x) = \frac{1}{2\pi}\sum_{n=0}^{N-1} b'_n e^{j(k_{x0}+n\Delta k)x} \quad (11)$$

$$h[m] = E_{\text{array,src}}\left(\frac{m\lambda}{2}\right), \quad m = 0 \text{ to } 4. \quad (12)$$

We verified our results with a full-wave simulation at 3 GHz using Ansoft HFSS. Fig. 4(a) shows the simulation scheme. Fig. 4(b) shows the simulated electric-field profile at the image plane, for the region $|x| \leq \lambda/2$, compared to theoretical calculation and the diffraction-limited sinc function. Again, the simulated electric field agrees extremely well with the calculated profile. The simulated E_y FWHM measures 0.37λ—identical to the free space case and significantly improved over the diffraction limit. While we have not shown the comparison in a figure, the amplitude of the subwavelength peak is about 11% of the peak of the sideband amplitude. This represents a 70% improvement over the free space case, which resulted because our placement of the extra zero worked toward decreasing the sideband amplitudes. This figure also compares quite favorably to other proposed superoscillation focusing schemes, such as the one proposed in [4], where a subwavelength peak with a similar focal width contains only 10^{-4} of the total power at the cross section of the focus. Fig. 4(c) shows typical variations in image profiles when we vary the excitation currents by a randomly phased white Gaussian component with mean amplitude 1% of the strongest excited current component. Despite the appearance of an uneven and increased sidelobe level, our achieved subwavelength focusing is unaffected by this level of perturbation. Our results show that: 1) one is able to tune the amplitude of the subwavelength peak relative to that of the sidelobes by changing the locations of zeros or introducing zeros; 2) it is possible to obtain a clear focusing improvement over the diffraction limit with reasonable sideband amplitudes; and 3) our proposed implementation can tolerate small variations in excitation currents. Further tradeoffs between focal width, peak amplitude, and device sensitivity can be facilitated by tuning zero locations, changing the number of spectral lines, and adjusting the spectral line spacing. This gives one the flexibility to tune subwavelength superoscillatory waveforms to specific applications of interest.

IV. Conclusion

We presented a method of designing a superoscillatory waveform via adapting the theory of superdirectivity. Using this method, we designed superoscillatory waveforms in two environments: a free space superoscillatory waveform implemented using a continuously varying source field distribution, and a waveguide superoscillatory waveform implemented using an array of five embedded line sources. In both cases, full-wave simulations agree extremely well with design calculations and verify the achievement of subwavelength foci 0.6 times that of the diffraction limit at five wavelengths away from the source. Both the focal width and the image distance can be further improved with power and sensitivity tradeoffs, thus bringing much flexibility to subwavelength focusing capabilities at the multiwavelength range.

References

[1] A. Grbic and G. V. Eleftheriades, "Overcoming the diffraction limit with a planar left-handed transmission-line lens," *Phys. Rev. Lett.*, vol. 92, p. 117403, Mar. 2004.
[2] A. Grbic, L. Jiang, and R. Merlin, "Near-field plates: Subdiffraction focusing with patterned surfaces," *Science*, vol. 320, pp. 511–513, Apr. 2008.
[3] F. M. Huang, N. Zheludev, Y. Chen, and F. J. G. De Abajo, "Focusing of light by a nanohole array," *Appl. Phys. Lett.*, vol. 90, p. 091119, Feb. 2007.
[4] F. M. Huang and N. I. Zheludev, "Super-resolution without evanescent waves," *Nano Lett.*, vol. 9, pp. 1249–1254, Jan. 2009.
[5] S. A. Schelkunoff, "A mathematical theory of linear arrays," *Bell Syst. Tech. J.*, vol. 22, pp. 80–107, Jan. 1943.
[6] H. G. Booker and P. C. Clemmow, "The concept of angular spectrum of plane waves, and its relation to that of polar diagram and aperture distributon," in *Proc. IEE*, 1950, vol. 97, pp. 11–17.
[7] P. J. S. G. Ferreira and A. Kempf, "Superoscillations: Faster than the Nyquist rate," *IEEE Trans. Signal Process.*, vol. 54, no. 10, pp. 3732–3740, Oct. 2006.
[8] H. J. Riblet and C. L. Dolph, "Discussion on "A current distribution for broadside arrays which optimizes the relationship between beam width and side-lobe level"," *Proc. IRE*, vol. 35, no. 5, pp. 489–492, May 1947.
[9] N. Yaru, "A note on super-gain antenna arrays," *Proc. IRE*, vol. 39, no. 9, pp. 1081–1085, Sep. 1951.
[10] F. Oberhettinger, *Tables of Fourier Transforms and Fourier Transforms of Distributions*. Berlin, Germany: Springer-Verlag, 1990, p. 21.